arXiv:1308.4177v1 [hep-ph] 19 Aug 2013

UCRHEP-533
August 2013

Supersymmetric Left-Right Model of Radiative Neutrino Mass with Multipartite Dark Matter

Subhaditya Bhattacharya [1], **Ernest Ma** [2], **and Daniel Wegman** [3]

Department of Physics and Astronomy, University of California, Riverside, California 92521, USA

Abstract

The unifiable supersymmetric left-right model where the neutral fermion n in the $SU(2)_R$ doublet $(n,e)_R$ is a dark-matter candidate, is shown to have the requisite particle content for the neutrino ν in the $SU(2)_L$ doublet $(\nu,e)_L$ to acquire a small radiative Majorana mass from dark matter, i.e. scotogenic from the Greek "scotos" meaning darkness. As a result, there are at least three coexisting stable dark-matter particles with different interactions. We study their possible phenomenological impact on present and future experiments.

[1]E-mail: subhaditya123@gmail.com
[2]E-mail: ma@phyun8.ucr.edu
[3]E-mail: wegman.daniel@gmail.com

1 Introduction

To understand dark matter in the context of extensions of the standard model of particle interactions, there are many avenues. Supersymmetry with $R-$parity conservation is the most common approach. Two other well-motivated scenarios have also been proposed in recent years. One is the idea of radiative neutrino mass induced by dark matter. The simplest such one-loop mechanism was proposed by one of us in 2006 [1]. It has been called "scotogenic" from the Greek "scotos" meaning darkness. This proposal has been studied and extended in a number of subsequent papers [2–17]. Another is to have a left-right extension where the neutral component n of the $SU(2)_R$ doublet $(n,e)_R$ is dark matter [18–23].

It was pointed out [22] that with the addition of new supermultiplets, the dark left-right model is unifiable with all gauge couplings converging at an energy scale of about 10^{16} GeV. These additional particles turn out to be exactly what are required for radiative neutrino masses in the scotogenic model [1]. Hence an opportunity exists for merging all three mechanisms for dark matter in the context of a supersymmetric unified theory of radiative neutrino masses. In this paper we will focus mainly on the dark matter (DM) phenomenology of this comprehensive model.

2 Model

Consider the gauge group $SU(3)_C \times SU(2)_L \times SU(2)_R \times U(1)$. A new global $U(1)$ symmetry S is imposed so that the spontaneous breaking of $SU(2)_R \times S$ will leave the combination $S' = S + T_{3R}$ unbroken. Under $SU(3)_C \times SU(2)_L \times SU(2)_R \times U(1) \times S \times M \times H$, where M and H are discrete Z_2 symmetries, with the usual R parity of the MSSM given by $R \equiv MH(-1)^{2j}$, the superfields transform as shown in Table 1. Because of supersymmetry, the Higgs sector is doubled, in analogy to the transition from the Standard Model (SM)

to the Minimal Supersymmetric Standard Model (MSSM). Another set of Higgs doublet superfields η and a new set of charged and neutral Higgs singlet superfields ζ are added to obtain gauge-coupling unification, as well as radiative seesaw neutrino masses.

Superfield	$SU(3)_C \times SU(2)_L \times SU(2)_R \times U(1)$	S	M	H
$\psi = (\nu, e)$	$(1, 2, 1, -1/2)$	0	$-$	$+$
$\psi^c = (e^c, n^c)$	$(1, 1, 2, 1/2)$	$-1/2$	$-$	$+$
N	$(1, 1, 1, 0)$	0	$-$	$-$
n	$(1, 1, 1, 0)$	1	$-$	$+$
$Q = (u, d)$	$(3, 2, 1, 1/6)$	0	$-$	$+$
$Q^c = (h^c, u^c)$	$(3^*, 1, 2, -1/6)$	$1/2$	$-$	$+$
d^c	$(3^*, 1, 1, 1/3)$	0	$-$	$+$
h	$(3, 1, 1, -1/3)$	-1	$-$	$+$
Δ_1	$(1, 2, 2, 0)$	$1/2$	$+$	$+$
Δ_2	$(1, 2, 2, 0)$	$-1/2$	$+$	$+$
Φ_{L1}	$(1, 2, 1, -1/2)$	0	$+$	$+$
Φ_{L2}	$(1, 2, 1, 1/2)$	0	$+$	$+$
Φ_{R1}	$(1, 1, 2, -1/2)$	$-1/2$	$+$	$+$
Φ_{R2}	$(1, 1, 2, 1/2)$	$1/2$	$+$	$+$
η_{L1}	$(1, 2, 1, -1/2)$	0	$+$	$-$
η_{L2}	$(1, 2, 1, 1/2)$	0	$+$	$-$
η_{R1}	$(1, 1, 2, -1/2)$	$1/2$	$+$	$-$
η_{R2}	$(1, 1, 2, 1/2)$	$-1/2$	$+$	$-$
ζ_1	$(1, 1, 1, -1)$	0	$+$	$-$
ζ_2	$(1, 1, 1, 1)$	0	$+$	$-$
ζ_3	$(1, 1, 1, 0)$	0	$+$	$-$

Table 1: Particle content of proposed model.

The superpotential of the model reads:

$$
\begin{aligned}
W &= -\mu_L \Phi_{L1}\Phi_{L2} - \mu_R \Phi_{R1}\Phi_{R2} - \mu_\Delta Tr(\Delta_1\Delta_2) \\
&- \mu_{L2}\eta_{L1}\eta_{L2} - \mu_{R2}\eta_{R1}\eta_{R2} - \mu_{s12}\zeta_1\zeta_2 - \mu_{s3}\zeta_3\zeta_3 \\
&+ f_1 \Phi_{L1}\Delta_2\Phi_{R2} + f_2 \Phi_{L2}\Delta_1\Phi_{R1} \\
&+ f_3 \eta_{L1}\Delta_1\eta_{R2} + f_4 \eta_{L2}\Delta_2\eta_{R1} + f_5 \Phi_{L1}\eta_{L1}\zeta_2 \\
&+ f_6 \Phi_{R1}\eta_{R1}\zeta_2 + f_7 \Phi_{L2}\eta_{L2}\zeta_1 + f_8 \Phi_{R2}\eta_{R2}\zeta_1 \\
&+ f_9 \Phi_{L1}\eta_{L2}\chi_3 + f_{10}\Phi_{L2}\eta_{L1}\zeta_3 \\
&+ f_{11}\psi\Delta_1\psi^c + f_{12} Q\Delta_2 Q^c + f_{13} Q\Phi_{L1} d^c \\
&+ f_{14} n\psi^c\Phi_{R1} + f_{15} h Q^c \Phi_{R2} \\
&+ f_{16}\psi N\eta_{L2} + f_{17}\psi^c N\eta_{R1}
\end{aligned} \tag{1}
$$

The symmetry $S \times M \times H$ is used here to distinguish ψ, Φ_{L1}, η_{L1} from one another, as well as ψ^c, Φ_{R2}, η_{R2}, and N, n, ζ_3. There are seven bilinear terms with coefficients μ and seventeen trilinear terms with coefficient f allowed by $S \times M \times H$.

Hence m_e comes from the $I_{3L} = 1/2$ and $I_{3R} = -1/2$ component of Δ_1, i.e. δ^0_{11} ($\langle\delta^0_{11}\rangle = u_1$) with $S' = 1/2 - 1/2 = 0$, m_u from the $I_{3L} = -1/2$ and $I_{3R} = 1/2$ component of Δ_2, i.e. δ^0_{22} ($\langle\delta^0_{22}\rangle = u_4$) with $S' = -1/2 + 1/2 = 0$, m_d from ϕ^0_{L1} ($\langle\phi^0_{L1}\rangle = v_{L1}$), m_n from ϕ^0_{R1} ($\langle\phi^0_{R1}\rangle = v_{R1}$), and m_h from ϕ^0_{R2} ($\langle\phi^0_{R2}\rangle = v_{R2}$). Note that ϕ^0_{L2} ($\langle\phi^0_{L2}\rangle = v_{L2}$) doesn't contribute to fermion masses, but is involved in the scalar and vector masses. This structure guarantees the absence of tree-level flavor-changing neutral currents.

3 Radiative seesaw neutrino masses

Since the neutrino ν does not couple to N through Φ_{L2}, it has no tree-level mass. However, the $\nu N \eta^0_{L2}$ and $\phi^0_{L1}\eta^0_{L2}\zeta_3$ couplings and the allowed Majorana masses for N and ζ_3 will

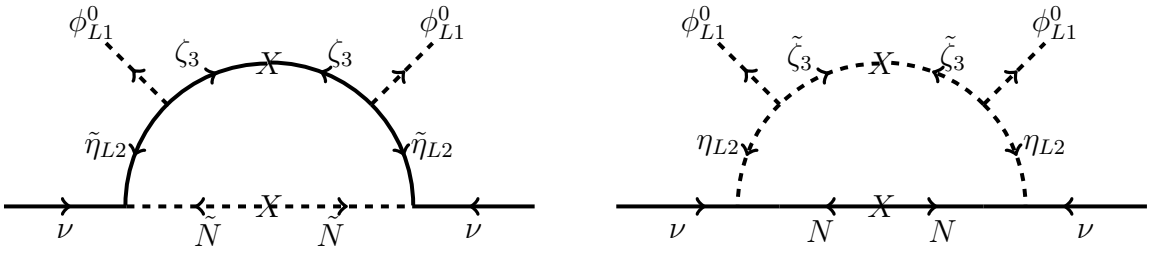


Figure 1: Scotogenic neutrino mass

generate one-loop radiative seesaw neutrino masses, as shown in Fig. 1.

The loop can be calculated exactly via

$$(M_\nu)_{\alpha\beta} = \sum_i \frac{h_{\alpha i} h_{\beta i} M_{Ni}}{16\pi^2} \left[\sum_j (U_R)_{1j} \left[\frac{m^2_{Rj}}{m^2_{Rj} - M^2_{Ni}} \ln \left(\frac{m^2_{Rj}}{M^2_{Ni}} \right) \right] - \sum_j (U_I)_{1j} \left[\frac{m^2_{Ij}}{m^2_{Ij} - M^2_{Ni}} \ln \left(\frac{m^2_{Ij}}{M^2_{Ni}} \right) \right] \right] \tag{2}$$

Where U_R (U_I) is the unitary matrix that makes $m_R(m_I)$ mass eigenstates and $h_{\alpha i}$ is the parameter for the interactions $\nu N \eta^0_{L2}$ and $\nu \tilde{N} {\tilde{\eta_{L2}}}^0$.

Both diagrams require supersymmetry breaking to be nonzero. The one on the right needs the A term $\phi^0_{L1}\eta^0_{L2}\tilde{\zeta}_3$ twice and the B term $\tilde{\zeta}_3\tilde{\zeta}_3$ once whereas the one on the left requires only the B term $\tilde{N}\tilde{N}$ once. We expect thus the latter diagram to be much more important. We estimate its contribution to be given by

$$m_\nu \simeq \frac{h^2 v^2_{L1} \Delta M^2_N}{16\pi^2 M^3_N}, \tag{3}$$

where h is the diagonal Yukawa coupling, ΔM^2_N is the supersymmetry breaking B term, and $M_3 \simeq M_N$ has been assumed. Using $v_{L1} \simeq 100$ GeV, $\Delta M^2_N \simeq 1$ TeV^2, and $M_N \simeq 10^5$ GeV, and $h^2 \simeq 10^{-3}$, we find $m_\nu \simeq 0.1$ eV.

4 Dark matter candidates of the model

There are three conserved quantities in this model: a global $U(1)$ number $S' = S + T_{3R}$, with $S' = 0$ for the usual quarks and leptons and $S' = 1$ for the scotino n, and the discrete Z_2 symmetries M and H. The usual R parity is then $R \equiv MH(-1)^{2j}$. The various superfields of this model under S', M, and H are listed in Table 2. A possible scenario for dark matter is

S'	M	H	Superfields
0	$-$	$+$	u, d, ν, e
0	$+$	$+$	$g, \gamma, W_L^{\pm}, Z, Z'$
0	$+$	$+$	$\phi_{L1}^0, \phi_{L1}^-, \phi_{L2}^+, \phi_{L2}^0, \phi_{R1}^0, \phi_{R2}^0$
0	$+$	$+$	$\delta_{11}^0, \delta_{11}^-, \delta_{22}^+, \delta_{22}^0$
1	$-$	$+$	n, h^c
-1	$-$	$+$	n^c, h
1	$+$	$+$	$W_R^+, \phi_{R2}^+, \delta_{12}^+, \delta_{12}^0$
-1	$+$	$+$	$W_R^-, \phi_{R1}^-, \delta_{21}^0, \delta_{21}^-$
0	$-$	$-$	N
0	$+$	$-$	$\eta_{L1}^0, \eta_{L1}^-, \eta_{L2}^+, \eta_{L2}^0, \eta_{R1}^-, \eta_{R2}^+$
0	$+$	$-$	$\zeta_1^-, \zeta_2^+, \zeta_3$
1	$+$	$-$	η_{R1}^0
-1	$+$	$-$	η_{R2}^0

Table 2: Superfields under $S' = S + T_{3R}$, M, and H.

to have the following three coexisting stable particles [24]: the lightest neutralino $\tilde{\chi}_1^0$ ($S' = 0$, $H = +$, $R = -$), the lightest scotino n ($S' = 1$, $H = +$, $R = +$), and the exotic $\tilde{\eta}_R^0$ fermion ($S' = 1$, $H = -$, $R = +$). One should note here that the $\tilde{\eta}_R^0$ fermion is a type of neutralino but, it doesn't mix with gauginos and other Higgsinos and that's how it differs from the lightest neutralino $\tilde{\chi}_1^0$ of this model, making it possible to be much heavier than the LSP and still be stable. However, there may be additional stable particles due to kinematics. For example, if the scalar counterpart of n cannot decay into n plus the lightest neutralino,

then it will also be stable. There may even be several exotic stable η and ζ particles. The dark sector may be far from just the one particle that is usually assumed, as in the MSSM. In the presence of several dark-matter candidates, the one with the largest annihilation cross section contributes the least, but may be the first to be discovered at the Large Hadron Collider (LHC). This means that in this model, the severe constraint due to dark-matter relic abundance on the one candidate particle of the MSSM, i.e. the lightest neutralino, may be relaxed, because it needs only to account for a fraction of the total dark-matter abundance. The allowed parameter space of the MSSM becomes much bigger and the opportunity for its discovery is enhanced at the LHC.

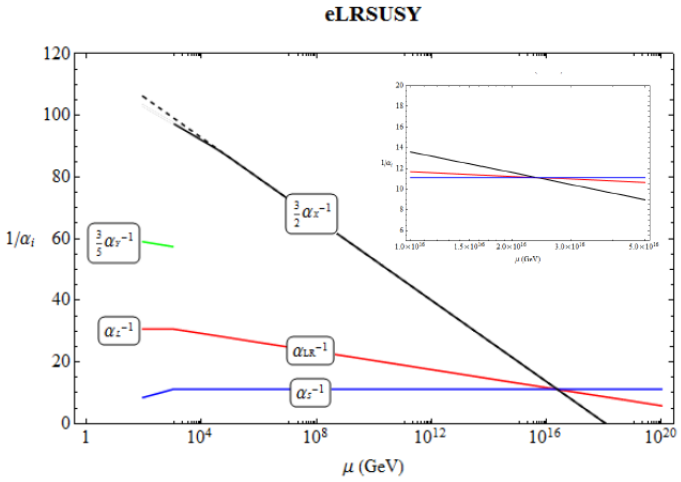


Figure 2: Gauge coupling unification in this model.

On Fig. 2, we show the gauge coupling unification of this model [22]. The $U(1)_Y$ coupling runs until the $SU(2)_R$ breaking scale M_R, where $\alpha_X^{-1}(M_R) = \alpha_Y^{-1}(M_R) + \alpha_L^{-1}(M_R)$ and $\alpha_L = \alpha_R$. After M_R, the gauge symmetry $SU(2)_L$ and $SU(2)_R$ are unified with a coupling α_{LR}. From the requirement of gauge-coupling unification, it was shown that if the $SU(2)_R$ breaking scale M_R equals to the supersymmetry breaking scale M_S, the mass scale

M_X of the singlet superfields $\zeta_{1,2,3}$ should obey

$$M_R^{7/4} M_X^{-3/4} \simeq 53.28 \text{ GeV}. \tag{4}$$

Given that the LHC has not seen any evidence of supersymmetry up to now, we can set $M_R \geq 1$ TeV. In that case, $M_X \geq 50$ TeV (the dashed line in Fig. 2 is included to easily observe the change of slope at M_X in the running of α_X). As a result, interactions involving $\zeta_{1,2,3}$ may be ignored in our studies of dark matter. We further assume that the $N_{1,2,3}$ singlets are also heavy, so they may also be ignored.

For our scenario, we assume the masses m_χ, m_n, m_η of the three stable dark-matter particles $\tilde{\chi}_1^0, n, \tilde{\eta}_R^0$ to be arranged in ascending order. $\tilde{\eta}_R^0$ has $I_{3L} = 0$, so it couples only to Z'. Hence the annihilation of $\tilde{\eta}_R^0 \bar{\tilde{\eta}}_R^0$ to Z' to particles with masses less than m_η will determine its relic abundance. Once $\tilde{\eta}_R^0$ freezes out, we need to consider the interactions of n. Again n has $I_{3L} = 0$, so it couples to Z', but there is also the interaction $\bar{e} n^c W_R^-$. Hence the annihilation of $n\bar{n}$ occurs through Z' to particles with mass less than m_n as well as to e^+e^- through $W_R^\pm$ exchange. This will determine the relic abundance of n. After n freezes out, the remaining particles are presumably those of the MSSM, and the annihilation of $\tilde{\chi}_1^0 \tilde{\chi}_1^0$ will determine its relic abundance.

This added flexibility should relax some of the most stringent constraints facing the MSSM today.

4.1 Bound on Z' from LHC data

Z' couples to the current [18, 21]

$$J_{Z'} = s_R^2 J_{3L} + c_L^2 J_{3R} - s_R^2 J_{em}, \tag{5}$$

with strength $g_{Z'} = e/s_R c_L \sqrt{c_L^2 - s_R^2}$. Given the unification requirements in [22], we assume, $g_L = g_R$ which implies, $\sin\theta_R = \sin\theta_L \equiv \sin\theta_W$. We evaluate the bound on the mass of

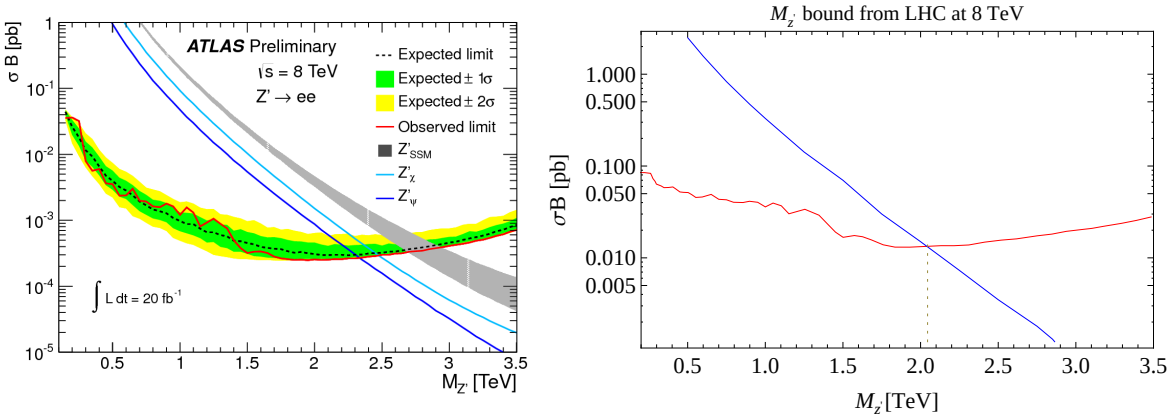


Figure 3: LHS: Bound on different Z' masses at LHC from ATLAS with $E_{CM} = 8$ TeV and integrated luminosity of 20 fb^{-1}. RHS: The limit is exploited to determine the bound on the Z' mass of this model.

Z' in our model from LHC data with $E_{CM} = 8$ TeV and integrated luminosity of 20 fb^{-1}. The result is shown in Fig 3. On the left, we show the figure from ATLAS [25], where the bound was obtained for producing Z' and subsequent decays to $e^{\pm}e^{\mp}$ for some popular Z' models. Right hand side shows our model cross-sections in blue and the bound from LHC data in red, as seen in the LHS of the figure. The cuts on the electron $p_T > 40$ GeV and pseudorapidity $|\eta| < 2.47$ has been employed to obtain the signal in our model. We use event generator `CalcHEP` [26] for calculating the cross-section and use `CTEQ6L` parton distribution function [27]. From Fig. 3 we obtain the bound on the mass of Z', $M_{Z'} = 2.045$ TeV $\simeq$ 2 TeV. The bound on SSM, the phenomenological Z' model with SM coupling, has been cross-checked to be around 2.8 TeV, as shown on the left hand side.

Gauge Boson masses are calculated to be:

$$\begin{aligned} M_Z &= \frac{g_L v_L}{\sqrt{2(1-2\sin^2\theta_W)}} \\ M_{Z'} &= M_Z\sqrt{\sin^2\theta_W + r^2\cos^2\theta_W} \\ M_{W_R} &= M_Z\sqrt{\sin^2\theta_W + r^2(\cos^2\theta_W - \sin^2\theta_W)} \end{aligned} \tag{6}$$

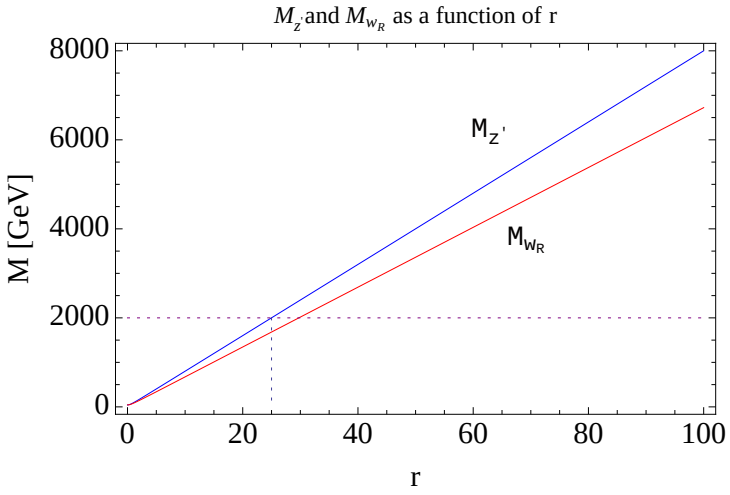


Figure 4: Linear dependence of $M_{Z'}$ (Blue) and M_{W_R} (Red) on the ratio of Higgs vevs r as defined in Eqn.7. A horizontal dotted line indicates the bound from LHC on Z' mass at 2 TeV.

Where $(v_L^2/u^2) = (1 - 2\sin^2\theta_W)/\sin^2\theta_W$ has been used to assume zero $Z - Z'$ mixing, and we have defined the ratio of Higgs vacuum expectation values as:

$$r = \frac{v_R}{v_L} \tag{7}$$

with $v_L^2 = v_{L1}^2 + v_{L2}^2, v_R^2 = v_{R1}^2 + v_{R2}^2$ and $u^2 = u_1^2 + u_4^2$.

In Fig. 4, we show the linear dependence of the Z' and W_R mass on the ratio of Higgs vacuum expectation values r following Eqn. 7. We note that mass of Z' is bigger than W_R for $M_Z' \geq 30$ GeV. The bound on $M_Z' \geq 2$ TeV from LHC eventually put a bound on $r \geq 25$ as shown. In the following analysis, we use r as a plotting variable instead of M_Z' or M_{W_R}.

4.2 Relic Abundance of n and $\tilde{\eta}_R^0$

The annihilation cross-sections for DM $\tilde{\eta}_R^0$ to SM particles goes through s-channel diagram exchanging Z', while n has an additional piece through a t-channel diagram to $e_R^\pm$ through $W_R^\pm$ exchange. The Feynman diagrams are shown in fig. 5 and 6.

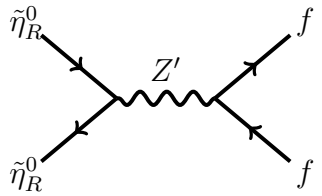


Figure 5: Feynman Diagram for $\tilde{\eta}_R^0$ annihilation to SM.

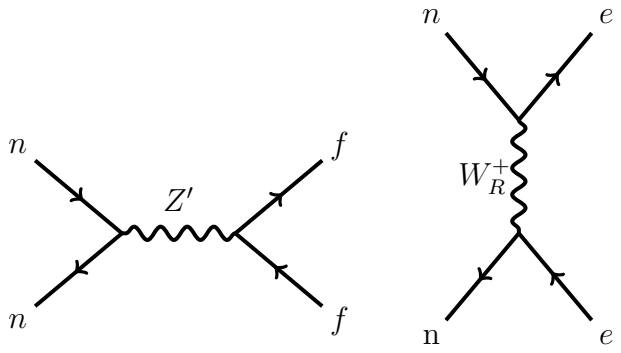


Figure 6: Feynman Diagram for n annihilation to SM.

The expressions for thermally averaged cross-section ($\langle\sigma v\rangle$) for these two DM components annihilating to SM are indicated in Eqn. 8 and Eqn. 9.

$$\langle\sigma v\rangle_\eta \simeq \frac{g_L^4}{64\pi}\frac{m^2_{\tilde{\eta}_R^0}}{(4m^2_{\tilde{\eta}_R^0}-M^2_{Z'})^2}\frac{(10-29c_W^2+22c_W^4)}{(2c_W^2-1)^2} \tag{8}$$

$$\langle\sigma v\rangle_n \simeq \frac{g_R^4 m_n^2}{64\pi}\Bigg[\frac{10s_W^4-9s_W^2c_W^2+3c_W^4}{(4m_n^2-M^2_{Z'})^2(c_W^2-s_W^2)^2} + \frac{3}{(m_n^2+M^2_{W_R})^2}+\frac{3(c_W^2-2s_W^2)}{(4m_n^2-M^2_{Z'})(m_n^2+M^2_{W_R})(c_W^2-s_W^2)}\Bigg] \tag{9}$$

With the unification condition, $g_R^2 = g_L^2 \simeq 0.427$ and $\sin^2\theta_W = 0.23$, numerically, we obtain:

$$\langle\sigma v\rangle_\eta \simeq \frac{0.00222 m_{\tilde{\eta}_R^0}{}^2}{4m_{\tilde{\eta}_R^0}{}^2 - M_Z'^2} \tag{10}$$

$$\langle\sigma v\rangle_n \simeq \frac{0.00222{m_n}^2}{4{m_n}^2 - M_Z'^2} + \frac{0.00272{m_n}^2}{{m_n}^2 + {M_{W_R}}^2} + \frac{0.00156{m_n}^2}{(4{m_n}^2 - M_Z'^2)({m_n}^2 + {M_{W_R}}^2)} \tag{11}$$

If we assume the decoupling of $\tilde{\eta}_R^0$, n and $\tilde{\chi}_1^0$ from the hot soup of SM particles are independent of interactions with each other, relic density for each DM component can be approximated as

$$\Omega_i h^2 \simeq \frac{0.1pb}{\langle\sigma v\rangle_i} \tag{12}$$

The total abundance will be a sum of the three DM components, i.e.

$$\Omega_{DM_{tot}} h^2 = \Omega_\eta h^2 + \Omega_n h^2 + \Omega_{\chi_1^0} h^2 \tag{13}$$

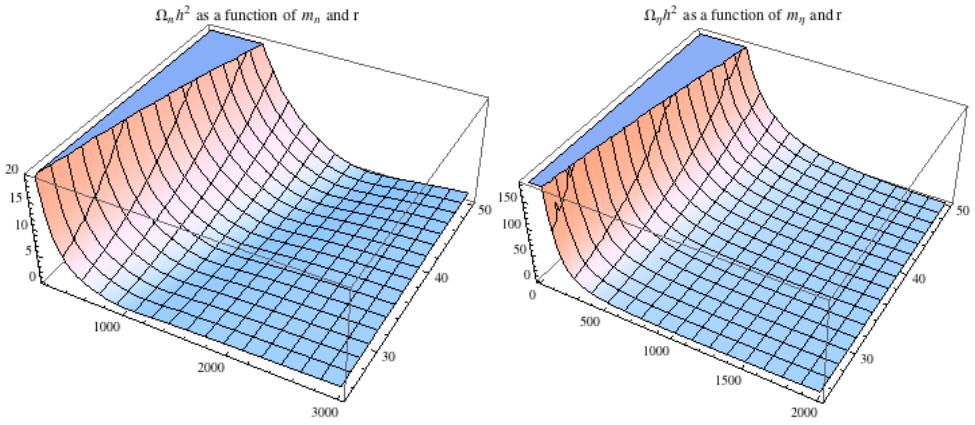


Figure 7: A 3-dim plot showing Ωh^2 (z-axis) dependence on mass (x-axis) and r (y-axis). LHS: n and RHS: $\tilde{\eta}_R^0$

With this assumption, we evaluate relic abundance for each of the DM component and look for the parameter space where they add up to the constraint from WMAP [28] [4].

$$0.094 < \Omega_{DM_{tot}} h^2 < 0.130 \tag{14}$$

[4] PLANCK [29] data essentially indicates a very similar range, though more stringent, almost indistinguishable from WMAP in present context.

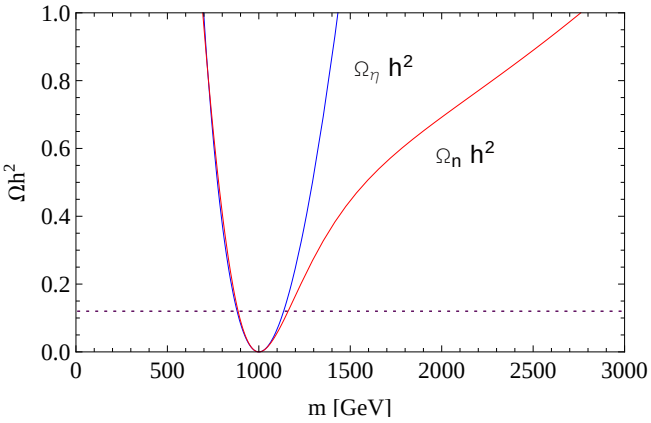


Figure 8: Ωh^2 dependence for DM n and $\tilde{\eta}_R^0$ on mass for r =25.

In Fig. 7, we show a 3-dimensional plot with Ωh^2 along z-axis, DM mass m along x-axis and the ratio of Higgs vevs r along y-axis for the DM component n on LHS and $\tilde{\eta}_R^0$ on RHS. We use Eqn 10, Eqn 11 and Eqn 12 to draw them. Both of the DMs show similar behaviour. Now, a cut along the r-axis at 25, shows the dependence of Ωh^2 on DM mass m which is shown in Fig 8. The difference in n and $\tilde{\eta}_R^0$ annihilation is clear from here.

In the three component DM framework, we study a scenario where the two components n and $\tilde{\eta}_R^0$ dominate in relic abundance leaving a very tiny space for neutralino $\tilde{\chi}_1^0$. We will discuss neutralino DM shortly. For example, we focus on a region of parameter space, where,

$$\Omega_\eta h^2 + \Omega_n h^2 = 0.1 \tag{15}$$

In such a case, if we assume in addition that each of the components contribute equally, then we end up getting Fig. 9. This indicates that we obtain two possible masses for a given value of r and Ωh^2 and the difference in n and $\tilde{\eta}_R^0$ annihilation doesn't matter in the range of r and Ωh^2 we are interested. This is shown in the top panel of Fig. 9, for n (left) and $\tilde{\eta}_R^0$ (right). They look exactly the same, where DM mass is plotted with r. In the bottom panel, we show the case when one of the components contribute fully to relic abundance with $\Omega_i h^2 = 0.1$.

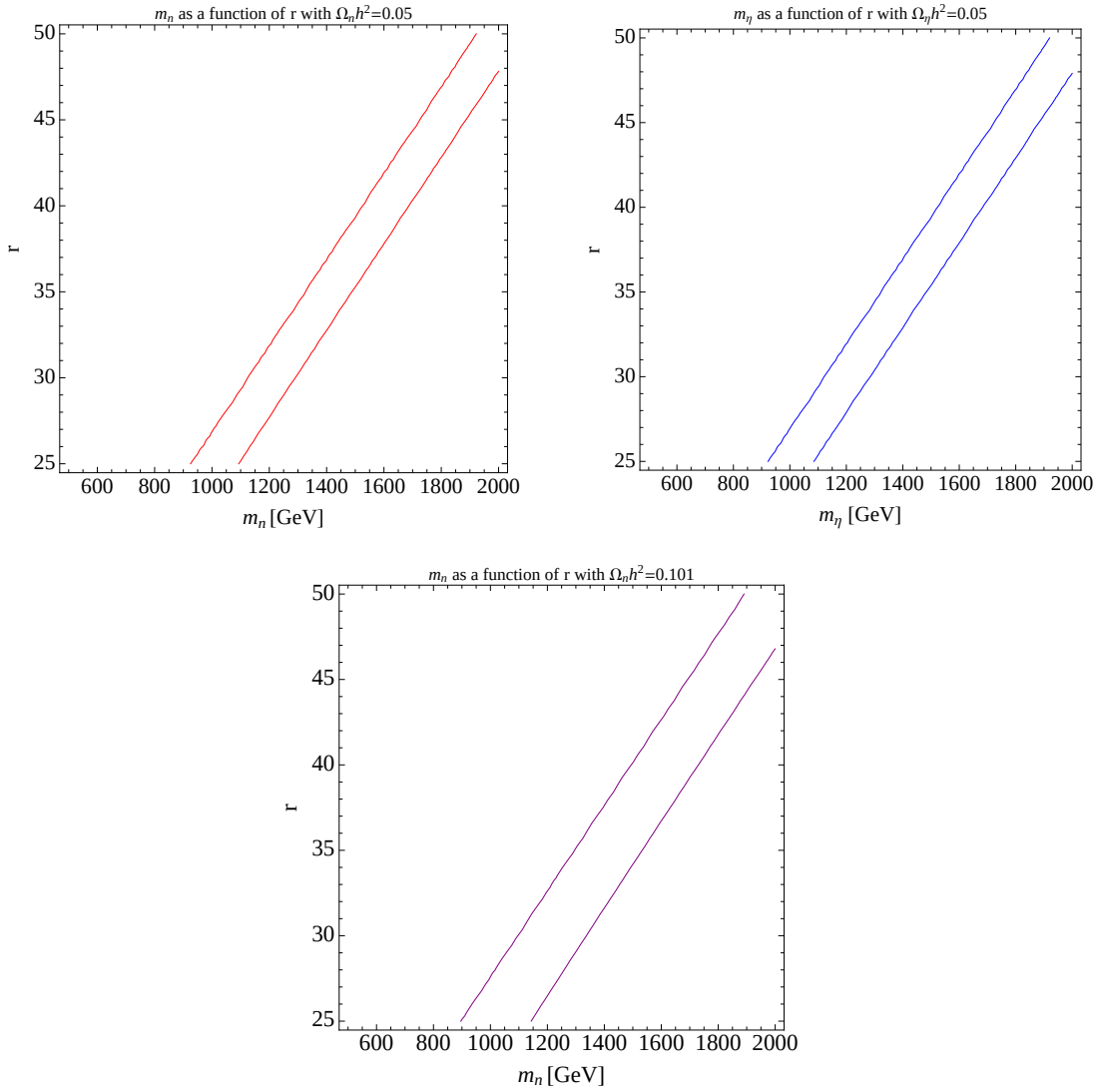


Figure 9: Top: $m-r$ dependence when each of the DM component n (left) and $\tilde{\eta}_R^0$ (right) DM contributing equally to the relic density with $\Omega_i h^2$ =0.05. Bottom: When one component dominates, i.e. $\Omega_i h^2$ =0.1. Masses are in GeVs.

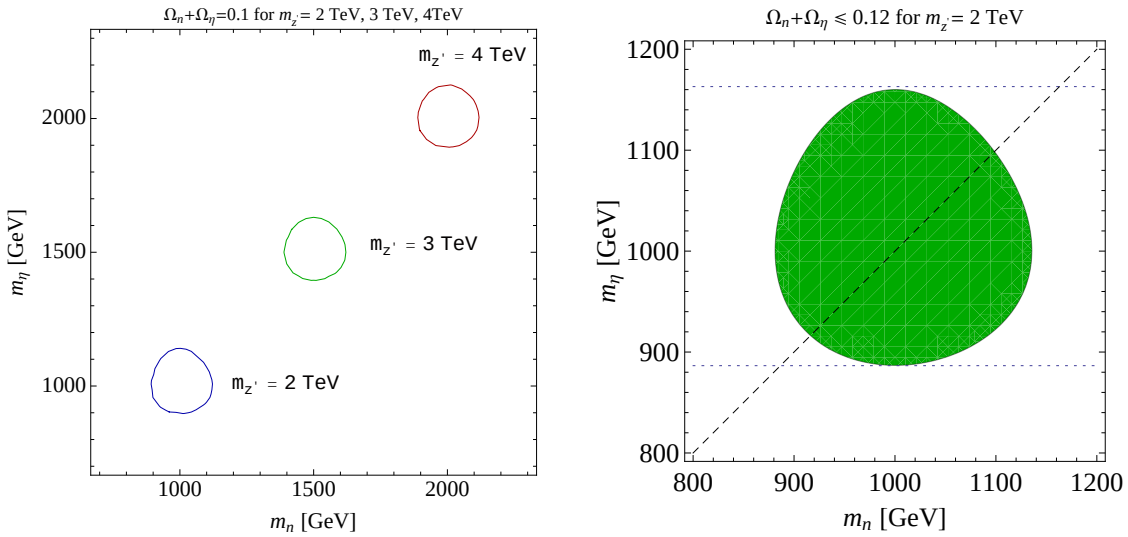


Figure 10: LHS: A plot showing m_n-m_η [GeV] contours for $\Omega_n h^2 + \Omega_\eta h^2$=0.1 for M'_Z = 2, 3, 4 TeV. RHS: Region of the m_n-m_η [GeV] parameter space when $\Omega_n h^2 + \Omega_\eta h^2 \leq$0.12 with M'_Z= 2 TeV.

Eqn. 15 is appropriately depicted in Fig. 10 for different Z' masses. They represent as three circles (The circular shape is understandable from looking at Fig. 8) in m_n and $m_{\tilde{\eta}^0_R}$ [GeV] plane for M'_Z = 2, 3 and 4 TeV around $m_n = m_{\tilde{\eta}^0_R} = M'_Z/2$. The reason is simple to understand; the resonance region essentially contributes for relic abundance. We highlight the case for $M'_Z = 2$ TeV in the RHS of Fig. 10. The whole region in green becomes allowed when we have the condition $\Omega_\eta h^2 + \Omega_n h^2 \leq 0.12$ (i.e. the contour shrinks for smaller abundance). We also note that, if we adhere to the assumption made initially that $m_\eta \geq m_n$, then only half of the circle above the diagonal line is allowed for relic abundance restricting the allowed mass range for n between 866-1100 GeV and for $\tilde{\eta}^0_R$ between 915-1163 GeV. Given that the plot is close to a perfect circle, $\Omega_n h^2 \geq \Omega_\eta h^2$ in this limit. Hence, if n and $\tilde{\eta}^0_R$ together contributes to 90% of the total dark matter relic density, $\tilde{\eta}^0_R$ can contribute in 1- 45% and n can contribute in 45-90%.

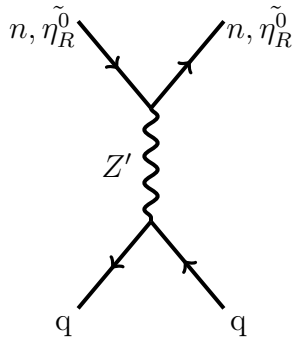


Figure 11: Diagram for scattering with quarks for direct detection.

4.3 Direct Detection of n and $\tilde{\eta}_R^0$

Direct detection of n and $\tilde{\eta}_R^0$ takes place through t-channel Z' interaction with quarks. The Feynman graph is shown in fig. 11. Due to only this contribution, the spin-independent (SI) cross-section is very small.

We use `MicrOMEGAs` [30] to calculate the effective SI nucleon scattering cross-section. The parton-level interaction is converted to the nucleon level by using effective nucleon ${f_q}^N$ $(N = p, n)$ couplings defined as [30]

$$\langle N|m_q\bar{\psi}_q\psi_q|N\rangle = {f_q}^N M_N\,, \tag{16}$$

where M_N is the nucleon mass and we use the default form factors in [30] as $f_u^p = 0.033,\ f_d^p = 0.023,\ f_s^p = 0.26$, for the proton; $f_u^n = 0.042,\ f_d^n = 0.018,\ f_s^n = 0.26$ for the neutron; while for the heavy quarks the f_q^N are generated by gluon exchange with the nucleon and are given by

$$f_Q^N = \frac{2}{27}\left(1 - \sum_{q=u,d,s} f_q^N\right) \quad Q = c, t, b. \tag{17}$$

The results are shown in Fig. 12. The bounds from XENON100 (above) and XENON1T (below) are shown in two continuous lines in purple and red respectively. Any points above

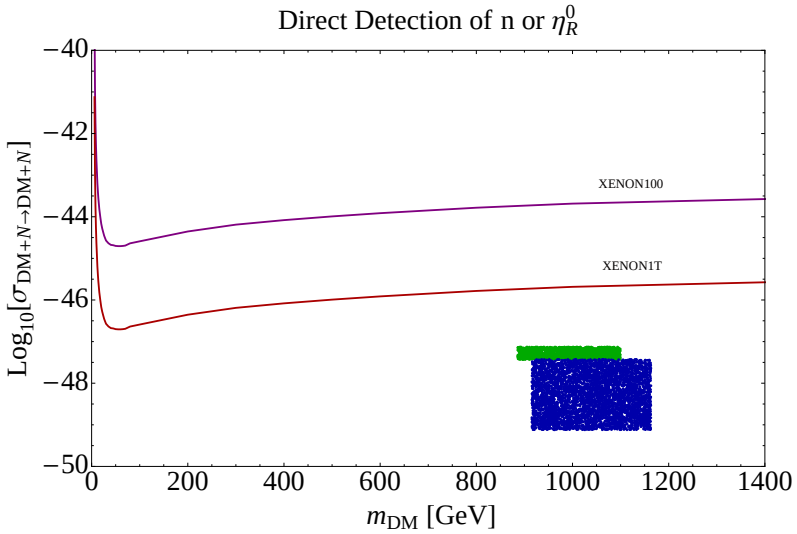


Figure 12: Direct detection constraint for DM n and $\tilde{\eta}_R^0$. Spin-independent effective nucleon cross-section [cm^2] in log scale is plotted in y-axis as a function of DM mass [GeV] along x-axis. The upper thick curve in purple shows the limit from XENON100 and the lower one in red is for XENON1T. Points in the blue box represents $\tilde{\eta}_R^0$ contributing 1-45 % (bottom to top) and those in green correspond to n contributing 45-90 % (bottom to top) of the total dark matter density in WMAP allowed mass range.

the XENON100 lines will be discarded by the direct search experiments. In Fig. 12, points in blue shows the results of SI direct detection cross-section for $\tilde{\eta}_R^0$ with M_Z'= 2 TeV and those in green represent n within the allowed mass range to obtain correct relic density; m_n between 866-1100 GeV and for m_η between 915-1163 GeV. Although n and $\tilde{\eta}_R^0$ have same quark interaction as in Fig. 11 and have same direct detection cross-section, given the mass hierarchy $m_\eta \geq m_n$, n contributes more than $\tilde{\eta}_R^0$ to the dark matter density. Due to multi-component nature of the dark matter, the effective direct detection cross-section for each DM component is obtained by multiplying the fraction of their number density $\frac{n_{DM}}{n_{tot}}$ with the actual nucleon cross-section σ_N (assuming that all of the DMs are accessible to the detector).

$$\sigma_{Neff} = \frac{n_{DM}}{n_{tot}}\sigma_N \simeq \frac{\Omega_{DM}h^2}{\Omega_{tot}h^2}\sigma_N \tag{18}$$

The thickness of the direct detection cross-section essentially comes from the fraction $\frac{n_{DM}}{n_{tot}}$, which has been varied between 1-45 % for $\tilde{\eta}_R^0$ (in blue) and 45-90% for n (in green). Hence, points at the bottom of the blue box constitute only 1% while those at the top in green constitute 90% of the total DM. The unequal thickness in blue and green box is due to the logarithmic scale of the effective cross-section.

The direct detection cross-section also doesn't depend on DM mass, while it depends on the Z' mass very much. With higher M'_Z they go down even below to make it harder for direct search. Possibility of early discovery of these DMs in near-future experiments seems to be small, although they are surely allowed by the exclusion limits set by XENON.

4.4 Relic Abundance and Direct detection of Wino type of Neutralino $\tilde{\chi}_1^0$

Let us now discuss the lightest neutralino ($\tilde{\chi}_1^0$) as the third DM candidates in this three-component DM set up. The neutralino sector in this extended LR SUSY model is non-trivial and constitutes of three gauginos (M_B, M_L, M_R) and thirteen Higgsinos. Seven out of them, which are superpartners of the scalar fields that do not have a vev, do not mix with the gauginos or the rest of the Higgsinos. This yields to a nine dimensional neutralino mass matrix.

For simplicity, we take a limit where the neutralino DM is predominantly a wino. In this limit, the neutralino of this model can easily mimic minimal supersymmetric Standard Model (MSSM) neutralino, with $M_B = M_1, \mu_L = \mu, \beta_L = \beta$,and $1.43M_L = M_2$. This is explicitly shown in the Appendix. In Fig. 13, we show as an example, that when μ_L (x-axis) is larger than M_L (which we set at 0.6 TeV), fraction of bino and Higgsino components in

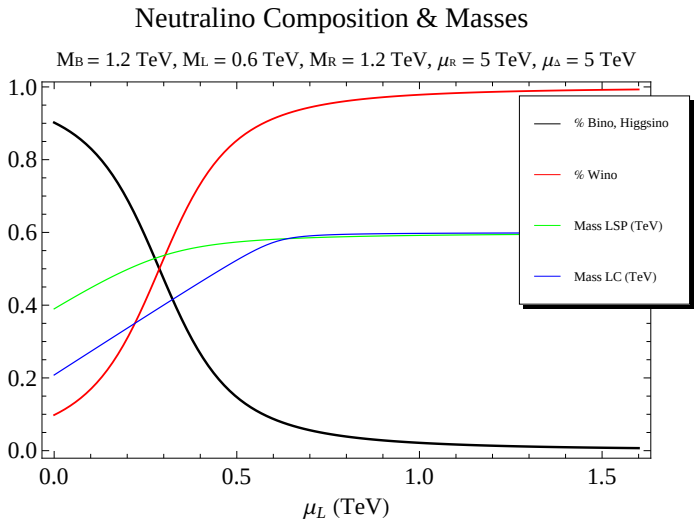


Figure 13: Plot showing a limit when the lightest neutralino becomes predominantly a Wino and the first chargino becomes degenerate with LSP.

lightest neutralino, in black thick line goes to almost zero; giving rise to a wino DM with the red line reaching 1. We also show that the lightest chargino (in blue, called LC) becomes degenerate with the lightest neutralino (in green) and both have mass around 600 GeV in this particular point in parameter space. This degeneracy is a very well known feature of wino dominated neutralino in MSSM. Note that in order to achieve this limit in this model, we kept $M_R \simeq M_B$ and other non-MSSM parts heavy, $\mu_R, \mu_\Delta = 5$ TeV.

It is also known that when lightest chargino is degenerate with neutralino DM, co-annihilation occurs [31], making $\tilde{\chi}_1^0$ annihilation cross-section much larger to yield very small abundance. This has been crafted in different ways [32–36] to make wino a viable DM candidate by having moduli decay in anomaly mediated SUSY breaking [33] or by non-thermal productions [36] etc. Wino DM has been studied also to justify PAMELA data [37]. However, the under-abundance works perfectly fine for us with the other two components to make up. Of course, other regions of neutralino DM parameter space where it is an admixture of Higgsino-wino-bino that yields under-abundance is also allowed for the model. We

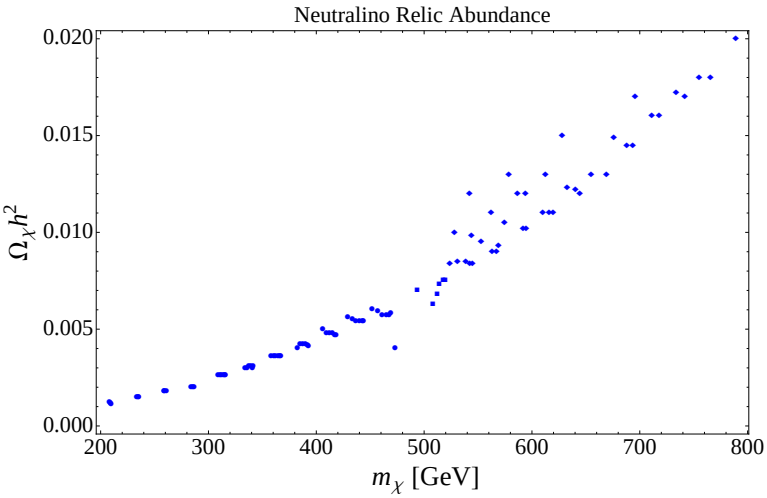


Figure 14: Relic Abundance of lightest neutralino as a function of mass when it is predominantly a wino. The scanned parameter space here ranges M_1: (800-1200) GeV, M_2: (200-775) GeV, μ: (600-1000) GeV with $\mu, M_1 > M_2$.

show a sample scan of wino dominated neutralino for relic density and direct detection. The MSSM parameter space scanned here: M_1 between 800-1200 GeV, $M_2 \simeq 1.43 M_L$, between 200-775 GeV, and the Higgsino parameter μ between 600-1000 GeV (with $\mu, M_1 > M_2$). In Fig 14, we show that the neutralino-DM under abundance for $\Omega_{\chi_1^0} h^2$ is not larger than 0.02 if we keep $m_{\tilde{\chi}_1^0} \leq 800$ GeV (This is following the assumption that neutralino is the lightest of the three DMs and the limit can be increased for higher Z' mass). The neutralino DM

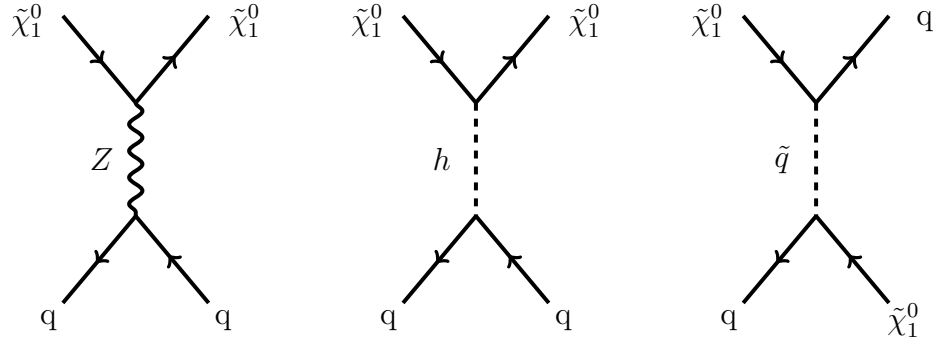


Figure 15: Diagram for lightest neutralino $\tilde{\chi}_1^0$ scattering with quarks for direct detection.

constitutes only 1%-20% of the total DM density making Eqn. 15 a good benchmark. Note that the scan yields a pre-dominantly wino, but with some Higgsino component in it.

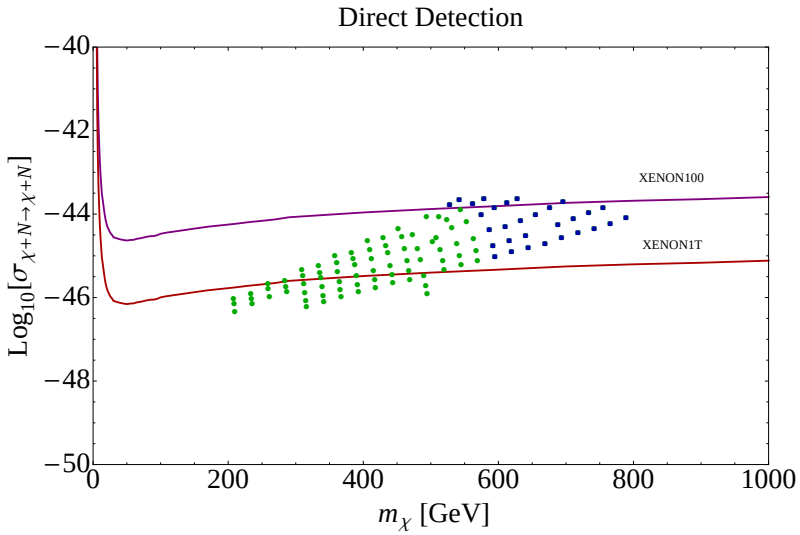


Figure 16: Direct detection constraint on neutralino DM mass when it is predominantly wino. The upper curve is for XENON100 and the lower one is for XENON1T. Points in blue have relic abundance more than 10% and those in green have less. Scanned parameter space ranges: M_1: (800-1200) GeV, M_2: (200-775) GeV, μ: (600-1000) GeV with $\mu, M_1 > M_2$.

We use MicrOMEGAs [30] to evaluate relic abundance and direct detection cross-sections for neutralino DM which mimics MSSM in the parameter space mentioned above. The direct detection cross-section for neutralino goes through t-channel processes as in Fig. 15. The squark contribution is negligible as they are heavy $\simeq$ 2 TeV. Also, for pure wino, there is no Higgs channel and the Z-channel contributes more to spin- dependent cross-section. Hence, having some Higgsino fraction in the neutralino enhance direct detection. in Fig. 16, we see that the neutralino can be accessible to direct detection experiments in near future with points close to XENON100 and XENON1T limit. Points in blue have relic abundance contribution with more than 10% and they have a early detection possibility while points in green have relic density less than 10% and direct detection for them may be delayed depending on the mass and composition. While higher order calculations for

direct detection of purely wino DM has been studied [38] to boost direct detection, we are not using them, since we are exploiting a small Higgsino fraction in the neutralino, that increases direct detection while having co-annihilations to yield under-abundance.

The mass range and the wino content in neutralino studied here is consistent with the indirect detection constraints from Fermi Gamma-Ray space telescope or the High Energy Spectroscopic System (H.E.S.S.) [39].

We also note that the MSSM parameter space scan performed here, doesn't correspond to a specific high-scale SUSY breaking pattern. So, the bounds on the chargino or neutralino masses obtained from LHC [40], which mostly assumes some specific high-scale pattern like minimal Supergravity (mSUGRA) [41], are not applicable here.

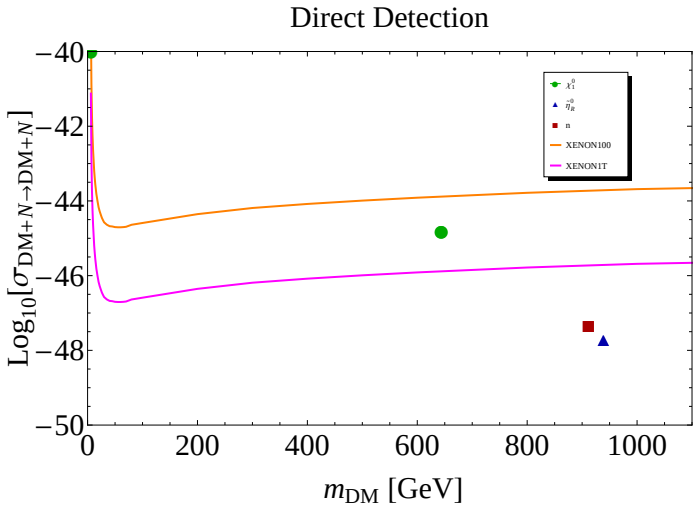


Figure 17: A sample point in the three component dark matter parameter space allowed by WMAP is plotted with respect to XENON100 and XENON1T limit. $\tilde{\chi}_1^0$ (644 GeV) in green, n (912 GeV) in red and $\tilde{\eta}_R^0$ (939 GeV) in blue constitutes 10.7%, 62.5% and 26.8% of total DM density respectively.

In Fig. 17, we show a sample point in the three component dark matter parameter space allowed by relic abundance with respect to XENON100 and XENON1T direct detection

limit. In this point $\tilde{\chi}_1^0$ (644 GeV) in green, n (912 GeV) in red and $\tilde{\eta}_R^0$ (939 GeV) in blue constitutes 10.7%, 62.5% and 26.8% of total DM density respectively.

5 Summary and Conclusions

In extended LR SUSY model three DM components can co-exist together: the lightest neutralino $\tilde{\chi}_1^0$, the lightest scotino n, and the exotic $\tilde{\eta}_R^0$ Higgsino. We show that in the limit of wino dominated $\tilde{\chi}_1^0$, thanks to the co-annihilation with chargino to yield under-abundance, the other two components contribute heavily to relic abundance, with masses m_n and m_η around 1 TeV that corresponds to the resonance annihilation with $m_{DM} \simeq M'_Z/2$. We found a bound on Z' from LHC to be at 2.045 TeV. With this value of M'_Z, the direct detection cross-section for n and $\tilde{\eta}_R^0$ is calculated to lie between $10^{-47} - 10^{-49}$ (cm^2)(depending on the fraction in which it contributes to total DM density). This is at least an order of magnitude smaller than XENON1T detection limits. Nevertheless, in such a multicomponent set up, a large wino dominated neutralino region becomes allowed without much complications while still obeying the existing limits and constraints; with appropriate parameters, $\tilde{\chi}_1^0$ does lie within the direct detection limits.

It is worthy to mention that the situation studied in this article is a simplification in the thermal history of three component DM set-up. Interaction of DM components (between n and $\tilde{\eta}_R^0$, which have been neglected given the specific mass hierarchy), can make the general situation more complicated and one needs to solve the coupled Boltzman equations corresponding to n, $\tilde{\eta}_R^0$ and $\tilde{\chi}_1^0$ to study the exact decoupling of each DM component depending on their relative masses and coupling strength.

The rich particle spectrum of this model with the right handed sector, makes it very likely to have interesting collider signatures at LHC by producing these new excitations. They also

open up new decay channels that may alter the final state event rates in the lepton or jet-rich final states with missing energy. This can serve as a distinctive feature of this model from MSSM and change the bounds on sparticle masses at LHC. We plan to elaborate on this in a future publication.

Acknowledgements:

This work is supported in part by the U. S. Department of Energy under Grant No. DE-FG03-94ER40837. The work of SB is supported by U.S Department of Energy under Grant No. DE-SC0008541. The work of DW is supported by UC MEXUS-CONACYT under Grant Reference No. 200406-303746.

Appendix

Using the basis

$$(\tilde{\Psi}^0)^T = \{\tilde{B}, \tilde{W}_L, \tilde{\phi}_{L1}, \tilde{\phi}_{L2}, \tilde{W}_R, \tilde{\delta}_{11}, \tilde{\delta}_{22}, \tilde{\phi}_{R1}, \tilde{\phi}_{R2}\}$$

The neutralino mass matrix in our model is :

$$M_{\chi^0} = \left(\begin{array}{cccc|cccc|c} M_B & 0 & -\frac{g_1 v_{L1}}{\sqrt{2}} & \frac{g_1 v_{L2}}{\sqrt{2}} & 0 & 0 & 0 & -\frac{g_1 v_{R1}}{\sqrt{2}} & \frac{g_1 v_{R2}}{\sqrt{2}} \\ 0 & M_L & \frac{g_L v_{L1}}{\sqrt{2}} & -\frac{g_L v_{L2}}{\sqrt{2}} & 0 & -\frac{g_L u_1}{\sqrt{2}} & \frac{g_L u_4}{\sqrt{2}} & 0 & 0 \\ -\frac{g_1 v_{L1}}{\sqrt{2}} & \frac{g_L v_{L1}}{\sqrt{2}} & 0 & -\mu_L & 0 & 0 & \frac{f_1 v_{R2}}{2} & 0 & \frac{f_1 u_4}{2} \\ \frac{g_1 v_{L2}}{\sqrt{2}} & -\frac{g_L v_{L2}}{\sqrt{2}} & -\mu_L & 0 & 0 & \frac{f_2 v_{R1}}{2} & 0 & \frac{f_2 u_1}{2} & 0 \\ \hline 0 & 0 & 0 & 0 & M_R & -\frac{g_R u_1}{\sqrt{2}} & \frac{g_R u_4}{\sqrt{2}} & \frac{g_R v_{R1}}{\sqrt{2}} & -\frac{g_R v_{R2}}{\sqrt{2}} \\ 0 & -\frac{g_L u_1}{\sqrt{2}} & 0 & \frac{f_2 v_{R1}}{2} & -\frac{g_R u_1}{\sqrt{2}} & 0 & -\mu_\Delta & \frac{f_2 v_{L2}}{2} & 0 \\ 0 & \frac{g_R u_4}{\sqrt{2}} & \frac{f_1 v_{R2}}{2} & 0 & \frac{g_R u_4}{\sqrt{2}} & -\mu_\Delta & 0 & 0 & \frac{f_1 v_{L1}}{2} \\ -\frac{g_1 v_{R1}}{\sqrt{2}} & 0 & 0 & \frac{f_2 u_1}{2} & \frac{g_R v_{R1}}{\sqrt{2}} & \frac{f_2 v_{L2}}{2} & 0 & 0 & -\mu_R \\ \frac{g_1 v_{R2}}{\sqrt{2}} & 0 & \frac{f_1 u_4}{2} & 0 & -\frac{g_R v_{R2}}{\sqrt{2}} & 0 & \frac{f_1 v_{L1}}{2} & -\mu_R & 0 \end{array}\right) \tag{19}$$

As mentioned in Section 4.3, this is also not the full matrix, but some elements are already decoupled form this matrix. It is important to note, $\tilde{B}$ is not the MSSM $U(1)_Y$ bino,

instead is a $SU(2)_R \times U(1)_Y$. But a linear combination of $\tilde{B}$ with $\tilde{W_R}$ in the limit $M_B \simeq M_R$ makes it a MSSM bino.

Defining the ratios $R_W = v_L/v_{SM} = \sqrt{\frac{1-2s_W^2}{1-s_W^2}} = 0.837$ and $\tan\beta_L = v_{L2}/v_{L1}$, we can rewrite the 4×4 upper left matrix in (19), with the basis $\left\{\tilde{B}, \tilde{W}, \tilde{\phi}_{L1}, \tilde{\phi}_{L2}\right\}$, (where $\tilde{W} = \frac{\tilde{W}_L}{R_W}$) as

$$M_{\chi^0_{MSSM}} = \begin{pmatrix} M_B & 0 & -M_Z * s_W * c_{\beta L} & M_Z * s_W * s_{\beta L} \\ 0 & \frac{M_L}{R_W^2} & M_Z * c_W * c_{\beta L} & -M_Z * c_W * s_{\beta L} \\ -M_Z * s_W * c_{\beta L} & M_Z * c_W * c_{\beta L} & 0 & -\mu_L \\ M_Z * s_W * s_{\beta L} & -M_Z * c_W * s_{\beta L} & -\mu_L & 0 \end{pmatrix} \tag{20}$$

This is exactly the MSSM neutralino mass matrix, where $M_B = M_1, \mu_L = \mu, \beta_L = \beta$,and $\frac{M_L}{R_W^2} \simeq 1.43 M_L = M_2$.

The rest of the Higgsinos in the basis, $\left(\tilde{\Psi_2}^0\right)^T = \{\eta^{\tilde{0}}_{L1}, \eta^{\tilde{0}}_{L2}, s^{\tilde{0}}_3\}$, $\left(\tilde{\Psi_3}^0\right)^T = \{\eta^{\tilde{0}}_{R1}, \eta^{\tilde{0}}_{R2}\}$ and $\left(\tilde{\Psi_4}^0\right)^T = \{\delta^{\tilde{0}}_{12}, \delta^{\tilde{0}}_{21}\}$ are

$$M_{H2} = \begin{pmatrix} 0 & -\mu_{L2} & f_{10} v_{L2} \\ -\mu_{L2} & 0 & f_9 v_{L1} \\ f_{10} v_{L2} & f_9 v_{L1} & -\mu_{s3} \end{pmatrix}, M_{H3} = \begin{pmatrix} 0 & -\mu_{R2} \\ -\mu_{R2} & 0 \end{pmatrix}, M_{H4} = \begin{pmatrix} 0 & -\mu_\Delta \\ -\mu_\Delta & 0 \end{pmatrix} \tag{21}$$

In the following basis:

$$(\Psi_1^+)^T = \{\imath\tilde{W}_L^+, \imath\tilde{W}_R^+, \tilde{\phi^+_{L2}}, \tilde{\delta^+_{22}}, \tilde{\phi^+_{R2}}, \tilde{\delta^+_{12}}\}$$
$$(\Psi_1^-)^T = \{\imath\tilde{W}_L^-, \imath\tilde{W}_R^-, \tilde{\phi^-_{L1}}, \tilde{\delta^-_{11}}, \tilde{\phi^-_{R1}}, \tilde{\delta^-_{21}}\}$$
$$(\Psi_2^+)^T = \{\tilde{\eta}^+_{L2}, \tilde{\eta}^+_{R2}, \zeta_2^+\}$$
$$(\Psi_2^-)^T = \{\tilde{\eta}^-_{L1}, \tilde{\eta}^-_{R1}, \zeta_1^-\}$$

The chargino mass matrices are:

$$M_{1\chi^{\pm}} = \begin{pmatrix} M_L & 0 & \frac{g_L v_{L2}}{2} & \frac{g_L u_4}{2} & 0 & 0 \\ 0 & M_R & 0 & \frac{g_R u_4}{2} & \frac{g_R v_{R2}}{2} & 0 \\ \frac{g_L v_{L1}}{2} & 0 & \mu_L & -f_1 v_{R2} & 0 & 0 \\ \frac{g_L u_1}{2} & \frac{g_R u_1}{2} & -f_2 v_{R1} & \mu_\Delta & 0 & 0 \\ 0 & \frac{g_R v_{R1}}{2} & 0 & 0 & \mu_R & -f_2 v_{L2} \\ 0 & 0 & 0 & 0 & -f_1 v_{L1} & \mu_\Delta \end{pmatrix} \tag{22}$$

$$M_{2\chi^{\pm}} = \begin{pmatrix} \mu_{L2} & f_3 u_1 & f_5 v_{L1} \\ f_4 u_4 & \mu_{R2} & f_6 v_{R1} \\ -f_7 v_{L2} & -f_8 v_{R2} & \mu_{s12} \end{pmatrix} \tag{23}$$

References

[1] E. Ma, Phys. Rev. **D73**, 077301 (2006).

[2] J. Kubo, E. Ma, and D. Suematsu, Phys. Lett. **B642**, 18 (2006).

[3] E. Ma, Mod. Phys. Lett. **A21**, 1777 (2006).

[4] E. Ma, Annales Fond. Broglie **31**, 285 (2006).

[5] E. Ma and U. Sarkar, Phys. Lett. **B653**, 288 (2007).

[6] T. Hambye, K. Kannike, E. Ma, and M. Raidal, Phys. Rev. **D75**, 095003 (2007).

[7] E. Ma, Phys. Lett. **B662**, 49 (2008).

[8] K. S. Babu and E. Ma, Int. J. Mod. Phys. **A23**, 1813 (2008).

[9] E. Ma, Mod. Phys. Lett. **A23**, 647 (2008).

[10] E. Ma, Mod. Phys. Lett. **A23**, 721 (2008).

[11] E. Ma, Phys. Lett. **B659**, 885 (2008).

[12] E. Ma and D. Suematsu, Mod. Phys. Lett. **A24**, 583 (2009).

[13] E. Ma, Phys. Rev. **D80**, 013013 (2009).

[14] E. Ma, Phys. Lett. **B671**, 366 (2009).

[15] Y. Farzan and E. Ma, Phys. Rev. **D86**, 033007 (2012).

[16] E. Ma, A. Natale, and A. Rashed, Int. J. Mod. Phys. **A27**, 1250134 (2012).

[17] E. Ma, Phys. Lett. **B717**, 235 (2012).

[18] S. Khalil, H.-S. Lee, and E. Ma, Phys. Rev. **D79**, 041701(R) (2009).

[19] E. Ma, Phys. Rev. **D79**, 117701 (2009).

[20] A. Aranda, J. L. Diaz-Cruz, J. Hernandez-Sanchez, and E. Ma, Phys. Rev. **D81**, 075010 (2010).

[21] S. Khalil, H.-S. Lee, and E. Ma, Phys. Rev. **D81**, 051702(R) (2010).

[22] E. Ma, Phys. Rev. **D81**, 117703 (2010).

[23] E. Ma, Phys. Rev. **D85**, 091701(R) (2012).

[24] Q.-H. Cao, E. Ma, J. Wudka, and C.-P. Yuan, arXiv:0711.3881 [hep-ph].

[25] ATLAS-CONF-2013-017, http://cds.cern.ch/record/1525524

[26] A. Belyaev, N. D. Christensen and A. Pukhov, Comput. Phys. Commun. **184**, 1729 (2013) [arXiv:1207.6082 [hep-ph]].

[27] H. L. Lai *et al.* [CTEQ Collaboration], Eur. Phys. J. C **12**, 375 (2000) [arXiv:hep-ph/9903282].

[28] G. Hinshaw *et al.* [WMAP Collaboration], arXiv:1212.5226 [astro-ph.CO].

[29] P. A. R. Ade *et al.* [Planck Collaboration], arXiv:1303.5076 [astro-ph.CO].

[30] G. Belanger, F. Boudjema, A. Pukhov and A. Semenov, Comput. Phys. Commun. **180**, 747 (2009) [arXiv:0803.2360 [hep-ph]].

[31] K. Griest and D. Seckel, Phys. Rev. D **43**, 3191 (1991).

[32] A. Birkedal-Hansen and B. D. Nelson, Phys. Rev. D **64**, 015008 (2001) [hep-ph/0102075].

[33] T. Moroi and L. Randall, Nucl. Phys. B **570**, 455 (2000) [hep-ph/9906527].

[34] H. Baer, A. Mustafayev, E. -K. Park and S. Profumo, JHEP **0507**, 046 (2005) [hep-ph/0505227]; H. Baer, T. Krupovnickas, A. Mustafayev, E. -K. Park, S. Profumo and X. Tata, JHEP **0512**, 011 (2005) [hep-ph/0511034].

[35] U. Chattopadhyay, D. Das, P. Konar and D. P. Roy, Phys. Rev. D **75**, 073014 (2007) [hep-ph/0610077].

[36] T. Moroi, M. Nagai and M. Takimoto, JHEP **1307**, 066 (2013) [arXiv:1303.0948 [hep-ph]].

[37] G. Kane, R. Lu and S. Watson, Phys. Lett. B **681**, 151 (2009) [arXiv:0906.4765 [astro-ph.HE]]; S. Mohanty, S. Rao and D. P. Roy, Int. J. Mod. Phys. A **27**, no. 6, 1250025 (2012) [arXiv:1009.5058 [hep-ph]].

[38] J. Hisano, S. Matsumoto, M. M. Nojiri and O. Saito, Phys. Rev. D **71**, 015007 (2005) [hep-ph/0407168]; J. Hisano, K. Ishiwata and N. Nagata, Phys. Lett. B **690**, 311 (2010) [arXiv:1004.4090 [hep-ph]].

[39] T. Cohen, M. Lisanti, A. Pierce and T. R. Slatyer, arXiv:1307.4082 [hep-ph].

[40] S. Eidelman *et al.* [Particle Data Group Collaboration], Phys. Lett. B **592**, 1 (2004).

[41] A. H. Chamseddine, R. Arnowitt and P. Nath, Phys. Rev. Lett. **49**, 970 (1982); R. Barbieri, S. Ferrara and C. A. Savoy, Phys. Lett. B **119**, 343 (1982); L. J. Hall, J. Lykken and S. Weinberg, Phys. Rev. D **27**, 2359 (1983); P. Nath, R. Arnowitt and A. H. Chamseddine, Nucl. Phys. B **227**, 121 (1983); N. Ohta, Prog. Theor. Phys. **70**, 542 (1983).